

# Learning to Localize in Unseen Scenes with Relative Pose Regressors

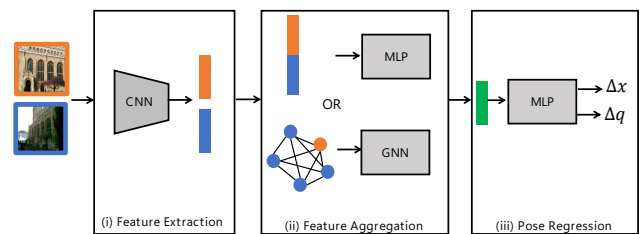
Ofer Idan, Yoli Shavit, Yosi Keller\*  
Bar Ilan University

## Abstract

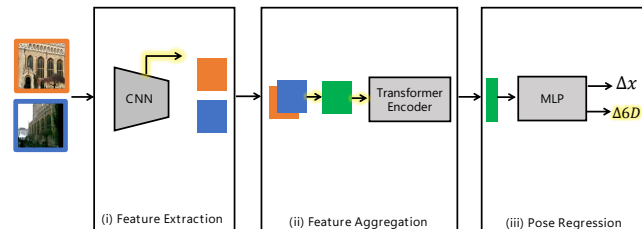
Relative pose regressors (RPRs) localize a camera by estimating its relative translation and rotation to a pose-labelled reference. Unlike scene coordinate regression and absolute pose regression methods, which learn absolute scene parameters, RPRs can (theoretically) localize in unseen environments, since they only learn the residual pose between camera pairs. In practice, however, the performance of RPRs is significantly degraded in unseen scenes. In this work, we propose to aggregate paired feature maps into latent codes, instead of operating on global image descriptors, in order to improve the generalization of RPRs. We implement aggregation with concatenation, projection, and attention operations (Transformer Encoders) and learn to regress the relative pose parameters from the resulting latent codes. We further make use of a recently proposed continuous representation of rotation matrices, which alleviates the limitations of the commonly used quaternions. Compared to state-of-the-art RPRs, our model is shown to localize significantly better in unseen environments, across both indoor and outdoor benchmarks, while maintaining competitive performance in seen scenes. We validate our findings and architecture design through multiple ablations. Our code and pretrained models is publicly available<sup>1</sup>.

## 1 Introduction

Image-based localization is an essential step in various computer vision applications, ranging from autonomous



(a) Relative Pose Regression Schemes



(b) Relative Pose Regression with Improved Generalization (Proposed)

Figure 1: Schemes for Relative Pose Regression.

navigation to positioning avatars in augmented or virtual reality. Some methods aim to tackle this problem using the query image alone. Scene coordinate regression (SCR) methods [6, 7] predict the 3D scene coordinates from the 2D pixels of the input image and then apply Perspective-n-Point (PnP) and RANSAC [17] to predict the camera pose. Absolute Pose Regression (APR) methods [25, 24, 37] directly regress the pose parameters from the query image. While offering fast and standalone solutions, both SCR and APR are confined by the absolute coordinates of the scenes and cannot generalize to unseen environments.

\*yosi.keller@gmail.com

<sup>1</sup><https://github.com/yolish/relformer>

Structure-based localization pipelines (SLPs) trade memory and speed for generalization, while achieving state-of-the-art localization accuracy in challenging conditions [41, 33, 34]. Extracting and matching global image descriptors, local features, and depth information allows establishing 2D-3D correspondences between query and visually similar reference images in order to estimate the camera pose using PnP and RANSAC. Since image retrieval, feature extraction, and feature matching are not scene-specific tasks, such pipelines can localize in new environments, without model retraining.

Relative Pose Regressors (RPRs) predict the parameters of the relative pose between a pair of cameras. Most contemporary RPRs first extract global features from query and reference images, using a convolutional backbone (Fig. 1a-i). The query and reference features are then joined and aggregated together (Fig. 1a-ii). Aggregation is typically performed through concatenation and one or more Fully Connected (FC) layers [26, 14, 4], or more recently, with Graphical Neural Networks (GNN) [44]. The resulting latent aggregation is passed to a multi-layer perceptron (MLP) which regresses the camera pose, typically represented with a 3D translation vector,  $\Delta x$ , and the quaternion parameterization of the relative rotation,  $\Delta q$  (Fig. 1a-iii). The pose of the query image is then computed by matrix inversion and multiplication. Some RPRs estimate instead the essential matrix and then apply RANSAC to estimate the pose of the query image [52].

Since RPRs learn to predict residuals, they can theoretically localize in scenes not seen during training ('unseen'). In practice, however, current methods present a significant degradation in performance in unseen environments [52, 44]. In this work, we study the generalization of RPRs. We consider the three main operations performed by relative pose regression methods: feature extraction, joint feature aggregation and pose regression. We find that operating on feature maps, available from intermediate activations, is key to localizing in unseen scenes (Fig 1b-i). Thus, we propose Relformer, an RPR model that concatenates, projects, and aggregates feature maps into latent codes using Transformer Encoders (Fig 1b-ii). We further adopt a recently proposed 6D representation for rotation matrices [53] for our learning objective, shown to be advantageous for regression tasks, compared to quaternions (Fig 1b-iii). We evaluate our method on indoor and outdoor benchmarks when local-

izing in 'seen' and 'unseen' environments. Relformer is shown to improve generalization to unseen scenes by a significant margin, compared to the current state-of-the-art RPRs, while achieving competitive performance on seen scenes.

In summary, our contributions are as follows:

- We show that operating on feature maps is key to improving the localization of RPRs in unseen scenes.
- We propose Relformer, a novel RPR architecture, which concatenates, projects, and aggregates feature maps with Transformer Encoders to predict the relative pose parameters.
- Our model surpasses current state-of-the-art RPRs in unseen environments, while maintaining competitive results on seen scenes.

## 2 Related Work

### 2.1 Visual Localization

Methods for image-based camera localization typically estimate the camera pose parameters in one of three ways: (1) with image retrieval (IR), (2) by establishing correspondences between 2D pixels and 3D scene coordinates and applying PnP-RANSAC (assuming known camera intrinsics) (3) by regressing explicit camera parameters from which the camera pose can be recovered (e.g., the camera pose parameters or a relative camera pose). IR methods [43, 1, 15, 31, 19] can localize images by taking the pose of the closest neighbor as the pose of the query image, or by interpolating the poses of several neighbors [21, 35]. Methods in the second class, often referred to as 'structure-based', include SLPs and SCR approaches. SLPs [41, 33, 34] find 2D-2D matches between the local features of the query and the reference images, obtained with IR, and then use depth labels to establish 2D-3D pairs. Instead of storing heavy-memory global and local image features, SCR methods [6, 7] directly regress the 3D world coordinates from the 2D pixels of the query image. Both SLPs and SCR achieve state-of-the-art localization accuracy. SLPs have high storage and runtime requirements, but can operate in challenging conditions and generalize to unseen scenes. SCR methods, in turn, are fast and estimate the camera pose using

the query image alone. However, they can only localize in scenes seen during training and need to be trained per scene. The last family of methods proposes to directly estimate camera parameters from images. APRs are typically trained per scene, encoding images with a convolutional backbone and then regressing the camera pose parameters with a multi-layer perceptron (MLP) [25, 23, 24, 28, 29, 48, 36]. This scheme was recently extended to learn multiple scenes with a single model using Transformers [38] or by indexing scene-specific weights [5]. Pose encoding was also proposed as a means for introducing scene priors and improving performance [39]. Relative pose regression methods regain generalization by learning the relative pose parameters instead of the absolute ones. Laskar et al. [26], were the first to suggest this approach using a Siamese ResNet34 backbone to encode a pair of images into global image descriptors and then regressed the relative pose parameters from their concatenation with an MLP. At test time, the model was applied to encode the query image and to regress the relative pose with respect to an image fetched from a reference database based on the distance between the query and reference encoding. The query camera pose was then estimated from the known pose of the reference image and the predicted relative pose, through matrix inversion and multiplication. The authors estimated pose candidates using several closest neighbors and then predicted the final pose through averaging algorithms. This approach was able to localize scenes not included in the model’s training set, albeit with a significant degradation in accuracy. Modifications to loss and training procedure were later proposed and achieved improved performance in seen environments [14, 4], matching or surpassing the accuracy of APRs. More recently, GNNs were suggested for exchanging information between multiple image encodings by learning and pruning the complete graph formed from the query and multiple neighbor images [44]. Instead of directly learning the relative pose parameters, Zhou et al. suggested learning the essential matrix from paired images [52] to recover the query camera pose. Other methods employed relative pose regression for estimating the motion with respect to a set of predicted anchor points [32] or to iteratively optimize an initial pose matrix by maximizing the similarity between the query image and the image synthesized with a neural radiance field [50] (pre-trained on the scene of interest). How-

ever, these approaches are scene-specific and, as opposed to RPRs, cannot localize in an unseen scene.

Compared to APRs, RPRs are slower and require the storage of image encodings. However, they achieve similar accuracy and can localize in unseen scenes. Compared to structured-based methods, RPRs (and regression approaches in general) present inferior localization accuracy. However, they are faster and have lower storage requirements than SLPs, while offering the ability to generalize to unseen scenes, which is lacking in SCR approaches. In practice, the performance of RPRs in unseen scenes significantly degrades compared to seen environments. In this work, we propose a method for improving the generalization of RPRs while maintaining performance in seen scenes.

## 2.2 Regressing Rotations with Deep Learning

RPRs typically regress the camera pose as a tuple  $\mathbf{p} :< \mathbf{x}, \mathbf{q} >$ , where  $\mathbf{x} \in \mathbb{R}^3$  gives the translation vector, and  $\mathbf{q} \in \mathbb{R}^4$  represents the unit quaternion parameterization of the camera rotation. The  $\mathbb{L}_2$  or  $\mathbb{L}_1$  losses are commonly used for optimizing the prediction of  $\mathbf{x}$  and  $\mathbf{q}$ , with respect to their ground truth values, and are joined together through manual [25, 36] or learned weights [24]. Brahmbhatt et al. [9] further proposed to use the log (unit) quaternion to improve performance. However, quaternions are not an optimal parameterization of rotation matrices. First, they suffer from an antipodal problem, where  $\mathbf{q}$  and  $-\mathbf{q}$  represent the same rotation matrix. Furthermore, it was recently shown that representations of 3D rotations in  $\leq 4$ D Euclidean real spaces are discontinuous [53]. Discontinuous representations, such as quaternions and Euler angles, were empirically shown to be inferior for regressing the rotation parameters, compared to continuous representations [53]. Consequently, different continuous representations for rotation regression were proposed [53, 27, 30, 12]. Zhou et al. [53] proposed learning a 6D vector, composed of the two first column vectors of the rotation matrix, and to recover the rotation matrix through a Gram-Schmidt orthogonalization process. Levinson et al. [27] instead suggested a 9D parameterization, which is based on the singular value decomposition (SVD) orthogonalization. In this work, we choose the 6D repre-

sentation for our learning objective (see the ablations in Tables 5,6,9).

### 2.3 Transformers in Visual Localization

Vaswani et al. [45] introduced transformers to encode and aggregate sequences with attention layers [3], in order to solve sequence-to-sequence problems in Natural Language Processing (NLP). Attention layers update each element in a sequence through weighted aggregation of all elements based on pairwise correlations. The attention mechanism is also related to bilinear pooling[51], which has been shown to improve image recognition at fine-grained levels.

Transformers were shown to outperform sequential neural models, such as RNNs and LSTMs in encoding long sequences, and were successfully applied for various tasks of natural language processing (NLP) and computer vision [13]. In the context of localization, Transformers were shown to achieve state-of-the-art performance for image retrieval [16], object detection[11], feature detection, extraction and matching [22, 40] and for multiscene absolute pose regression [37].

Encouraged by a recent observation that hybrid architectures of CNN and Transformers outperform CNN- and Transformer-Only architectures [49] and the success of Transformers in learning camera pose regression[37], we propose a novel CNN-Transformer RPR architecture which aggregates paired feature maps into latent representations of relative pose parameters.

## 3 Method

We implement our method using the hybrid CNN-Transformer architecture, we call Relformer, which is depicted in Fig. 2. We apply a shared convolutional backbone to extract feature maps from image pairs and apply two separate branches to predict the translation and rotation parameters, respectively. Each branch is implemented with a Transformer Encoder and an MLP head. The Transformer Encoders aggregate paired feature maps, extracted from query and reference images, into a latent representation of the pose parameters. Each MLP head regresses its target ( $\Delta_x$  or  $\Delta 6D$ ) from the respective latent representation.

### 3.1 Feature Extraction

Given a pair of images  $\mathbf{I}_1, \mathbf{I}_2 \in \mathbb{R}^{H \times W \times C}$ , we apply a Siamese convolutional backbone to extract feature maps. Similarly to [38], we extract a feature map per regression target:  $\mathbf{F}_{\text{trans}}^i$  and  $\mathbf{F}_{\text{rot}}^i$ , for learning translations and rotations, respectively (for image  $i=1, 2$ )

### 3.2 Paired Feature Aggregation

The extracted feature maps capture visual information from each image. Given the feature maps  $\mathbf{F}_t^1, \mathbf{F}_t^2 \in \mathbb{R}^{H_f \times W_f \times C_f}$ , extracted for learning the regression target  $\mathbf{t}$  from the pair  $\mathbf{I}_1, \mathbf{I}_2$ , we compute a *paired* feature map  $\mathbf{F}_t \in \mathbb{R}^{H_f \times W_f \times C_h}$  by applying channelwise concatenation and linear projection with a  $1 \times 1$  convolution (projecting to dimension  $C_h$ ). We also assign an encoding to each position in our paired feature map. Specifically, we learn a 2D position encoding as in [11], by defining the embedding vectors  $\mathbf{E}_x \in \mathbb{R}^{(W_f+1) \times C_h/2}$  and  $\mathbf{E}_y \in \mathbb{R}^{(H_f+1) \times C_h/2}$ , such that a position  $(i, j)$ ,  $i \in 1..H_f, j \in 1..W_f$ , is encoded by the concatenation of the corresponding embedding vectors:

$$\mathbf{E}_{pos}^{i,j} = \begin{bmatrix} \mathbf{E}_x^j \\ \mathbf{E}_y^i \end{bmatrix} \in \mathbb{R}^{C_h}. \quad (1)$$

The paired feature map and its position encoding are then flattened into a sequence  $\widehat{\mathbf{F}}_t \in \mathbb{R}^{H_f \cdot W_f \times C_h}$ .

In order to aggregate our sequence into a latent vector representation, we follow recent methods for sequence classification [13], and append a learned task token  $\mathbf{r}_t \in \mathbb{R}^{C_h}$  to the flattened feature map  $\widehat{\mathbf{F}}_t$ . The pose token is assigned to the position  $(0, 0)$  and the embedding vectors  $(\mathbf{E}_x^0, \mathbf{E}_y^0)$  and is appended to the position encoding sequence. Therefore, the input to the Transformer Encoder learning task  $\mathbf{t}$  is given by:  $[\mathbf{r}_t, \widehat{\mathbf{F}}_t] \in \mathbb{R}^{(H_f \cdot W_f + 1) \times C_h}$ .

We use the Transformer-Encoder architecture implementation of [11], which includes  $n$  identical Encoder layers. Each layer consists of a multi-head self-attention (MHA) module and an MLP with two layers and gelu non-linearity. The learned position encoding is added to the input before applying each Transformer Encoder layer. A LayerNorm [2] is applied before each module (MHA/MLP) and the input is added to the output with residual connections [45] and dropout. We take the output of the encoder at the position of the special token:

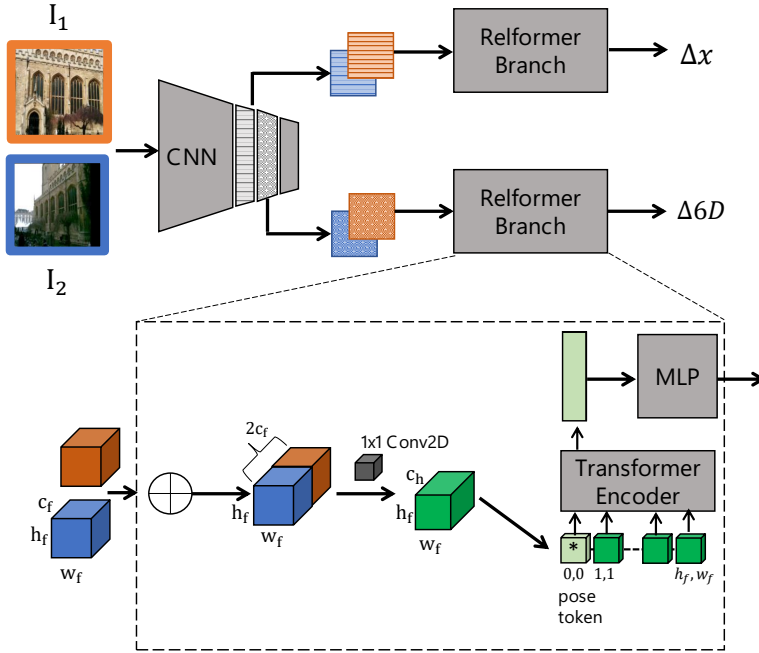


Figure 2: The architecture of our proposed model (Relformer).

$\mathbf{r}_t' \in \mathbb{R}^{C_h}$ , which aggregates the information from the entire paired sequence.

### 3.3 Pose Regression

We apply an MLP with a single hidden layer and gelu non-linearity to regress the target vector of task  $\mathbf{t}$  from  $\mathbf{r}_t'$ . Specifically, we regress  $\Delta \mathbf{x} \in \mathbb{R}^3$ , the translation vector, and  $\Delta \mathbf{6D} \in \mathbb{R}^6$ , the 6D parameterization of the rotation matrix  $\Delta \mathbf{R} \in \mathbb{R}^{3 \times 3}$ . Given the known pose of  $\mathbf{I}_1 : \langle \mathbf{x}_1, \mathbf{R}_1 \rangle$ , we can recover the pose of  $\mathbf{I}_2$  using  $\Delta \mathbf{x}$  and  $\Delta \mathbf{R}$ :

$$\mathbf{x}_2 = \mathbf{x}_1 + \Delta \mathbf{x}, \mathbf{R}_2 = \mathbf{R}_1 \Delta \mathbf{R}, \quad (2)$$

### 3.4 Training Loss for Relative Camera Pose

We optimize our model with the pose loss suggested by [24] for learning the relative weights of the translation and

rotation losses  $L_{\Delta \mathbf{x}}$  and  $L_{\Delta \mathbf{6D}}$ :

$$L_p = L_{\Delta \mathbf{x}} \exp(-s_{\Delta \mathbf{x}}) + s_{\Delta \mathbf{x}} + L_{\Delta \mathbf{6D}} \exp(-s_{\Delta \mathbf{6D}}) + s_{\Delta \mathbf{6D}}, \quad (3)$$

where  $s_{\Delta \mathbf{x}}$  and  $s_{\Delta \mathbf{6D}}$  are learned parameters.  $L_{\Delta \mathbf{x}}$  and  $L_{\Delta \mathbf{6D}}$  are given by the  $\mathbb{L}_1$  norm of the difference between the predicted and ground truth values. We recover the rotation matrix from the predicted 6D representation using Gram-Schmidt orthogonalization [53].

## 4 Experimental Results

This work focuses on studying and improving the generalization of RPRs. Hence, we evaluated our model's performance by localizing previously seen and unseen indoor and outdoor contemporary benchmarks, used to evaluate regression methods. We compare our results to recent state-of-the-art relative pose regression methods (Tables 1, 2, 3) and also provide a broader comparative analysis, across different classes of localization (Table 4). We further carry out ablations in order to assess the partic-

Table 1: **Localizing with RPRs in indoor previously seen scenes (7Scenes)**. We report the median position and orientation errors (in meters/degrees, respectively) for each scene and the average of the medians in all scenes. The best and second-best results are highlighted (in bold/underline, respectively).

Method	Chess	Fire	Heads	Office	Pumpkin	Kitchen	Stairs	Avg.
NN-Net[26]	0.13/6.50	0.26 /12.7	<u>0.14/12.3</u>	0.21/7.40	0.24/6.40	0.24/8.00	0.27/11.8	0.21/9.30
RelocNet[4]	0.12/4.10	0.26 /10.4	<u>0.14/10.5</u>	0.18/5.30	0.26/4.20	0.23/5.10	0.28/7.50	0.21/6.70
CamNet[4]	-/-	-/-	-/-	-/-	-/-	-/-	-/-	<b>0.05, 1.80</b>
EssNet [52]	0.13/5.10	0.27/10.1	<u>0.15/9.90</u>	0.21/6.90	0.22/6.1	0.23/6.90	0.32/11.2	0.22/8.00
NC-EssNet [52]	0.12/5.60	0.26 /9.60	<u>0.14/10.7</u>	0.20/6.70	0.22/5.70	0.22/6.30	0.31/7.90	0.21/7.50
RelPoseGNN [44]	<b>0.08/2.70</b>	<b>0.21 /7.50</b>	<b>0.13/8.70</b>	<b>0.15/4.10</b>	<b>0.15/3.50</b>	<b>0.19/3.70</b>	<b>0.22/6.50</b>	<u>0.16/5.20</u>
<b>Relformer (Ours)</b>	<u>0.11/4.01</u>	<u>0.23/8.57</u>	0.17/10.9	<u>0.16/4.92</u>	<u>0.15/4.15</u>	<u>0.19/4.89</u>	<u>0.24/6.46</u>	0.18/6.27

Table 2: **Localizing with RPRs in unseen scenes (7Scenes)**. The methods were trained with training sets of six scenes and evaluated on the remaining scene. We report the median position and orientation errors (in meters/degrees, respectively) for each scene and the average of medians across all scenes. Results for methods marked with ‘\*\*’ were reported and reproduced by [44]. The best and second-best results are highlighted (with bold/underline, respectively).

Method	Chess	Fire	Heads	Office	Pumpkin	Kitchen	Stairs	Avg.
NN-Net[26]*	0.33/ <b>11.5</b>	11.68 / <b>13.8</b>	0.30/15.5	1.34/ <b>10.9</b>	<u>0.41/12.8</u>	1.68/12.9	0.44/ <u>13.6</u>	2.31/13.0
EssNet[52]*	0.73/37.6	0.89/67.6	0.62/28.5	0.84/36.3	1.06/33.3	0.91/36.1	1.19/42.1	0.89/40.2
NC-EssNet[52]*	0.62/24.2	0.75/23.7	0.44/25.6	0.88/28.0	1.02/24.5	0.77/20.8	1.25/36.5	0.82/26.2
RelPoseGNN[44]	<u>0.29/12.8</u>	<u>0.45/15.7</u>	<b>0.19/14.7</b>	<u>0.42/12.5</u>	0.44/11.7	<u>0.42/12.4</u>	<b>0.35/15.5</b>	<u>0.36/13.6</u>
<b>Relformer (Ours)</b>	<b>0.27/8.49</b>	<b>0.34/10.4</b>	<u>0.28/12.1</u>	<b>0.32/8.24</b>	<b>0.40/9.06</b>	<b>0.32/9.23</b>	<u>0.42/10.5</u>	<b>0.34/9.72</b>

Table 3: **Localizing with RPRs in outdoor previously seen and unseen environments (Cambridge Landmarks)**. We report the average of the median position and orientation errors (in meters/degrees, respectively) when training on the CambridgeLandmarks dataset (Seen) and when training on the 7Scenes dataset (Unseen). In both cases, the models are evaluated on four scenes from the Cambridge Landmarks dataset. The best and second-best results are highlighted (in bold/underline, respectively).

Method	Seen	Unseen
EssNet [52]	1.07/3.42	10.4/85.8
NC-EssNet [52]	<u>0.84/2.83</u>	<u>7.98/24.4</u>
RelPoseGNN [44]	<b>0.91/2.3</b>	-/-
<b>Relformer (Ours)</b>	1.33/3.52	<b>3.35/10.6</b>

ular contribution of the main building blocks of our architecture to the performance and generalization of our model (Table 5,6). In addition, we evaluate different design choices: the convolutional backbone used (Table 7),

the dimension of the feature maps (Table 8) and the rotation parameterization (Table 9).

**Datasets.** The 7Scenes dataset [18] describes a small-scale indoor environment ( $\sim 1 - 10m^2$ ), captured inside an office building. It consists of seven scenes and presents various localization challenges such as motion blur, reflections, occlusions and repetitive textures. The CambridgeLandmarks dataset [25] is a mid-scale dataset ( $\sim 900 - 5500m^2$ ), captured in an urban outdoor environment. The dataset presents challenges that are typical to outdoor localization, such as changing lighting conditions and variations in scale, view points and trajectory. We evaluated our model in four (of six) scenes, which are commonly used as benchmarks by regression methods.

**Training Details.** We follow the training procedure of [38] and apply the augmentation method suggested by [25]. Specifically, during training, images are first rescaled such that their smaller edge is resized to 256 pixels. We extract random  $224 \times 224$  crops and randomly jitter the brightness, saturation, and contrast. At test time,



images are rescaled, and the center crop is used for inference, with no further augmentations. Our model is optimized using Adam, with  $\beta_1 = 0.9$ ,  $\beta_2 = 0.999$  and  $\epsilon = 10^{-10}$  and a batch size of 8. We used an initial learning rate of  $\lambda = 10^{-4}$  and a weight decay of  $10^{-4}$  and trained for 30 (600) epochs for indoor (outdoor) localization. Our loss is initialized as in [24]. The training pairs for the 7Scenes dataset are generated as in [14]. We further extend this dataset with pairs from [26]. Pairs from the CambridgeLandmarks dataset are computed by encoding images with a pre-trained NetVLAD model [1], and fetching the nearest 40 neighbors based on cosine similarity. At train time, we sample from the pool of neighbors to generate different pairs. We provide the training pairs, code, configuration files, and pre-trained models in order to support the reproducibility of our results. All models were trained on a single NVIDIA RTX A5000 24GB GPU.

**Implementation Details.** We use EfficientNet-B0 [42] as our convolutional backbone. We extract the feature maps  $\mathbf{F}_{\text{trans}}$  and  $\mathbf{F}_{\text{rot}}$  at resolutions of  $14 \times 14 \times 112$  and  $28 \times 28 \times 40$ , respectively, as these endpoints were previously shown to provide useful features for camera pose regression [37] (we reconfirm this choice in our ablation study). We set  $C_h = 512$  for the dimension of our projected paired feature maps and their respective positional encoding. Our Transformer Encoder is implemented with a standard architecture consisting of six layers and a dropout of  $p = 0.1$ . Each layer contains a MHA module with eight heads and an MLP which expands the input dimension (512) to 2048 with a hidden layer and gelu non-linearity and then decrease it back to 512 with another FC layer. Our MLP regressor heads preserve the dimension of the input and then regress the target with an FC layer. Evaluation on the 7Scenes dataset is done using the pairs (query and reference image) from [26], in line with [44]. For the CambridgeLandmarks dataset, for each query, we fetch the nearest neighbor using a pre-trained NetVLAD model [1].

#### 4.1 Localization in Seen and Unseen Scenes

Tables 1,2 compare the median position and orientation errors of our model (Relformer) and recent state-of-the-art RPRs for localizing the 7Scenes dataset. We consider localization in seen scenes, where the training data contain

images from all seven scenes (Table 1) and localization in unseen scenes (Table 2), where each time we train on six scenes and report the pose error for the remaining unseen scene. Relformer consistently outperforms current state-of-the-art RPRs when localizing in unseen scenes, while maintaining competitive performance for seen scenes. In particular, we note a significant improvement in regressing the rotation in unseen scenes. Table 3 reports the average of median position and orientation errors for the CambridgeLandmarks dataset. We observe a similar trend, where our model achieves a significant improvement in unseen scenes, while performing similarly to other methods in seen scenes. We also consider a broader comparative analysis in order to examine the different tradeoffs exhibited by different localization approaches. Table 4 compares representative methods from different localization families: IR, SLP, SCR, APR and RPR. Methods in the SLP and SCR families achieve state-of-the-art localization. The SLP approach enables accurate localization in unseen scenes, but is slow and requires large storage. SCR methods, on the other hand, are fast and light but need to be trained per scene and fail to generalize in unseen scenes. Regression methods are less accurate than the SOTA SLP and SCR approaches. APRs and RPRs perform similarly on seen scenes. APRs are faster than RPRs and do not require extra storage, but, as opposed to RPRs, they cannot localize in unseen scenes. Hence, the key upside of RPRs over APRs is in their ability to generalize to unseen scenes. Within the family of localization-by-regression (absolute and relative pose regression), our model localizes better in unseen scenes while outperforming APR approaches and maintaining competitive results compared to contemporary RPRs.

#### 4.2 Ablation Study

We study the particular contributions of the main algorithmic components of our model, differentiating it from contemporary RPRs (see Fig. 1): feature maps (FM), paired aggregation with a Transformer Encoder (TE) and a 6D rotation representation as a regression target (6D). Tables 5 and 6 report position and orientation errors when localizing in seen and unseen scenes from the 7Scenes dataset, respectively. Our baseline architecture (first row in Tables 5 and 6), extracts global descriptors instead of feature maps (1280-dimensional vectors), concatenates them

and passes them to two dedicated MLP heads to regress the translation and rotation parameters (with the same architecture as the MLP heads used in our fully proposed model). We also compare our full architecture to a configuration where feature maps are aggregated with two 2D convolution layers and relu non-linearity after concatenation and projection (second row in Tables 5 and 6). Our full model and the latter two configurations are trained using the Loss in Eq. 3 with the quaternion representation. We compare their performance to our full Relformer configuration, which uses the 6D rotation parameterization. The use of a Transformer Encoder to aggregate feature maps and the adoption of 6D parameterization have resulted in a notable improvement in orientation estimation, as demonstrated in Table 5. The use of feature maps instead of a global descriptor computed through average pooling, together with the proposed paired aggregation, leads to improved position estimation. A similar trend is observed when localizing in unseen scenes, and such algorithmic components can be adopted by other relative pose regression methods to improve their generalization. Table 7 further studies the choice of the backbone used to extract feature maps. We report the performance for the Fire scene, when aggregating the features with a 2D convolution (the same configuration as in the second row of Tables 5 and 6). To allow for a fair comparison, we consider feature maps with the same height and width. The Efficient-B0 backbone achieves the best position and orientation errors for both seen and unseen scenarios. Interestingly, we observe that features from the same backbone type (ResNet[20]) with a higher dimension yield better performance when the scene is seen during training but degrade the generalization of the model, compared to more compact features of the same resolution (ResNet50 versus ResNet34, respectively). Finally, we also validate two main aspects of our architecture design: the aggregation operation on different dimensions of the extracted feature maps (Table 8) and the parameterization of the rotation (Table 9). Consistent with our other experiments, we observe that the aggregation of flattened paired feature maps, while attending to nearby and long-range correlations (Transformer Encoder) yields better results, compared to local aggregation with 2D convolutions (Table 8). This trend is consistent for different feature maps. Extracting the  $14 \times 14$  and  $28 \times 28$  resolution for learning the translation- and rotation-related features with Trans-

former Encoders achieves better performance compared to the other configuration tested. When comparing models trained with different rotation parameterizations (Table 9), we find that the 6D representation achieves the lowest orientation error on average, with a consistent improvement of  $\sim 0.5^\circ$  between scenes. We note that the continuous parameterizations tested (6D and 9D) yield better results compared to representation by quaternions, which is consistent with the findings of [53].

### 4.3 Limitations and Future Work

We note that, while our model outperforms other regression methods in unseen scenes, its generalization differs greatly for position and orientation. For example, when examining the orientation errors for unseen scenes in the 7Scenes dataset, our model not only significantly improves the performance compared to other methods, but also achieves an error that is similar in magnitude to the error achieved in previously seen scenes. For position estimation, however, the improvement is minor and the degradation between seen and unseen scenes is larger. We attribute that to the different visual cues required to predict translation and rotation. Rotation estimation is more scale-invariant and can rely on cues such as lines and shadows even without significant visual overlap [10]. However, the estimation of translations requires some knowledge of the scene scale. Whether this can be mitigated through further research or is an inherent limitation of RPRs, is a topic for future research. In addition, we note that our method requires larger storage compared to current relative pose regression methods, since feature maps, instead of global descriptors, need to be saved. This limitation can potentially be mitigated by compression and reconstruction.

## 5 Conclusions

We presented a novel approach for relative pose regression, which pairs and aggregates feature maps with Transformer Encoders. Our model surpasses current regression methods in unseen scenes while maintaining competitive localization in seen scenes. Through multiple ablations across indoor and outdoor benchmarks, we show that attention-based aggregation of paired feature maps is



key for improving the localization of RPRs. In addition, we take advantage of recent advances in rotation representation and learn a modified parameterization of the camera pose, which reduces the orientation errors of our model. Our proposed approach is modular and can be adopted by RPRs in order to improve their performance and generalization.

## References

- [1] R. Arandjelović, P. Gronat, A. Torii, T. Pajdla, and J. Sivic. Netvlad: Cnn architecture for weakly supervised place recognition. *IEEE Transactions on Pattern Analysis and Machine Intelligence*, 40(6):1437–1451, 2018. 2, 7
- [2] Jimmy Lei Ba, Jamie Ryan Kiros, and Geoffrey E Hinton. Layer normalization. *arXiv preprint arXiv:1607.06450*, 2016. 4
- [3] Dzmitry Bahdanau, Kyunghyun Cho, and Yoshua Bengio. Neural machine translation by jointly learning to align and translate. In *Proceedings of the International Conference on Learning Representations (ICLR)*, 2015. 4
- [4] Vassileios Balntas, Shuda Li, and Victor Prisacariu. Relocnet: Continuous metric learning relocalisation using neural nets. In *Proceedings of the European Conference on Computer Vision (ECCV)*, September 2018. 2, 3, 6
- [5] Hunter Blanton, Connor Greenwell, Scott Workman, and Nathan Jacobs. Extending absolute pose regression to multiple scenes. In *IEEE Conference on Computer Vision and Pattern Recognition Workshops (CVPRW)*, pages 38–39, 2020. 3, 12
- [6] E. Brachmann, A. Krull, S. Nowozin, J. Shotton, F. Michel, S. Gumhold, and C. Rother. DSAC - differentiable RANSAC for camera localization. In *Proceedings of the IEEE/CVF Conference on Computer Vision and Pattern Recognition (CVPR)*, pages 2492–2500, Los Alamitos, CA, USA, jul 2017. 1, 2, 12
- [7] E. Brachmann and C. Rother. Learning less is more - 6d camera localization via 3d surface regression. In *Proceedings of the IEEE/CVF Conference on Computer Vision and Pattern Recognition (CVPR)*, pages 4654–4662, 2018. 1, 2, 12
- [8] Eric Brachmann and Carsten Rother. Visual camera relocalization from rgb and rgb-d images using dsac. *IEEE Transactions on Pattern Analysis and Machine Intelligence*, 44(9):5847–5865, 2021. 12
- [9] Samarth Brahmabhatt, Jinwei Gu, Kihwan Kim, James Hays, and Jan Kautz. Geometry-aware learning of maps for camera localization. In *Proceedings of the IEEE/CVF Conference on Computer Vision and Pattern Recognition (CVPR)*, 2018. 3
- [10] Ruojin Cai, Bharath Hariharan, Noah Snavely, and Hadar Averbuch-Elor. Extreme rotation estimation using dense correlation volumes. In *Proceedings of the IEEE/CVF Conference on Computer Vision and Pattern Recognition (CVPR)*, 2021. 8
- [11] Nicolas Carion, Francisco Massa, Gabriel Synnaeve, Nicolas Usunier, Alexander Kirillov, and Sergey Zagoruyko. End-to-end object detection with transformers. In *Proceedings of the European Conference on Computer Vision (ECCV)*, pages 213–229, Cham, 2020. 4
- [12] Jiayi Chen, Yingda Yin, Tolga Birdal, Baoquan Chen, Leonidas J Guibas, and He Wang. Projective manifold gradient layer for deep rotation regression. In *Proceedings of the IEEE/CVF Conference on Computer Vision and Pattern Recognition (CVPR)*, pages 6646–6655, 2022. 3
- [13] Jacob Devlin, Ming-Wei Chang, Kenton Lee, and Kristina Toutanova. BERT: Pre-training of deep bidirectional transformers for language understanding. In *Proceedings of the 2019 Conference of the North American Chapter of the Association for Computational Linguistics: Human Language Technologies, Volume 1*, pages 4171–4186, Minneapolis, Minnesota, June 2019. 4
- [14] Mingyu Ding, Zhe Wang, Jiankai Sun, Jianping Shi, and Ping Luo. CamNet: Coarse-to-fine retrieval for camera re-localization. In *Proceedings of the IEEE International Conference on Computer Vision (ICCV)*, October 2019. 2, 3, 7
- [15] M. Dusmanu, I. Rocco, T. Pajdla, M. Pollefeys, J. Sivic, A. Torii, and T. Sattler. D2-net: A trainable cnn for joint description and detection of local features. In *Proceedings of the IEEE/CVF Conference on Computer Vision and Pattern Recognition (CVPR)*, pages 8084–8093, 2019. 2
- [16] Alaaeldin El-Nouby, Natalia Neverova, Ivan Laptev, and Hervé Jégou. Training vision transformers for image retrieval. *arXiv preprint arXiv:2102.05644*, 2021. 4
- [17] Martin A. Fischler and Robert C. Bolles. Random sample consensus: A paradigm for model fitting with applications to image analysis and automated cartography. *Commun. ACM*, 24(6):381–395, June 1981. 1
- [18] B. Glocker, S. Izadi, J. Shotton, and A. Criminisi. Real-time rgb-d camera relocalization. In *2013 IEEE International Symposium on Mixed and Augmented Reality (ISMAR)*, pages 173–179, 2013. 6
- [19] Stephen Hausler, Sourav Garg, Ming Xu, Michael Milford, and Tobias Fischer. Patch-netvlad: Multi-scale fusion of locally-global descriptors for place recognition. In *Proceedings of the IEEE/CVF Conference on Computer*

- Vision and Pattern Recognition (CVPR)*, pages 1414–14152, 2021. 2
- [20] K. He, X. Zhang, S. Ren, and J. Sun. Deep residual learning for image recognition. In *Proceedings of the IEEE/CVF Conference on Computer Vision and Pattern Recognition (CVPR)*, pages 770–778, 2016. 8
- [21] Martin Humenberger, Yohann Cabon, Noé Pion, Philippe Weinzaepfel, Donghwan Lee, Nicolas Guérin, Torsten Sattler, and Gabriela Csurka. Investigating the role of image retrieval for visual localization. *International Journal of Computer Vision*, 2022. 2
- [22] Wei Jiang, Eduard Trulls, Jan Hosang, Andrea Tagliasacchi, and Kwang Moo Yi. COTR: Correspondence Transformer for Matching Across Images. In *Proceedings of the IEEE International Conference on Computer Vision (ICCV)*, 2021. 4
- [23] Alex Kendall and Roberto Cipolla. Modelling uncertainty in deep learning for camera relocalization. In *Proceedings of the IEEE International Conference on Robotics and Automation (ICRA)*, pages 4762–4769, 2016. 3, 12
- [24] A. Kendall and R. Cipolla. Geometric loss functions for camera pose regression with deep learning. In *Proceedings of the IEEE/CVF Conference on Computer Vision and Pattern Recognition (CVPR)*, pages 6555–6564, 2017. 1, 3, 5, 7, 12
- [25] A. Kendall, M. Grimes, and R. Cipolla. Posenet: A convolutional network for real-time 6-dof camera relocalization. In *Proceedings of the IEEE International Conference on Computer Vision (ICCV)*, pages 2938–2946, 2015. 1, 3, 6, 12
- [26] Z. Laskar, I. Melekhov, S. Kalia, and J. Kannala. Camera relocalization by computing pairwise relative poses using convolutional neural network. In *Proceedings of the IEEE International Conference on Computer Vision Workshops (ICCVW)*, pages 920–929, 2017. 2, 3, 6, 7, 12
- [27] Jake Levinson, Carlos Esteves, Kefan Chen, Noah Snavely, Angjoo Kanazawa, Afshin Rostamizadeh, and Ameesh Makadia. An analysis of svd for deep rotation estimation. *Advances in Neural Information Processing Systems (NIPS)*, 33:22554–22565, 2020. 3, 13
- [28] Iaroslav Melekhov, Juha Ylioinas, Juho Kannala, and Esa Rahtu. Image-based localization using hourglass networks. In *Proceedings of the IEEE International Conference on Computer Vision Workshops (ICCVW)*, pages 870–877, 2017. 3
- [29] Tayyab Naseer and W. Burgard. Deep regression for monocular camera-based 6-dof global localization in outdoor environments. *Proceedings of the IEEE/RSJ Conference on Intelligent Robots and Systems (IROS)*, pages 1525–1530, 2017. 3
- [30] Valentin Peretroukhin, Matthew Giamou, David M Rosen, W Nicholas Greene, Nicholas Roy, and Jonathan Kelly. A smooth representation of belief over so (3) for deep rotation learning with uncertainty. *arXiv preprint arXiv:2006.01031*, 2020. 3
- [31] Filip Radenović, Giorgos Tolias, and Ondřej Chum. Fine-tuning cnn image retrieval with no human annotation. *IEEE Transactions on Pattern Analysis and Machine Intelligence*, 41(7):1655–1668, 2018. 2
- [32] Soham Saha, Girish Varma, and CV Jawahar. Improved visual relocalization by discovering anchor points. *Proceedings of the British Machine Vision Conference*, 2018. 3
- [33] P. Sarlin, C. Cadena, R. Siegwart, and M. Dymczyk. From coarse to fine: Robust hierarchical localization at large scale. In *Proceedings of the IEEE/CVF Conference on Computer Vision and Pattern Recognition (CVPR)*, pages 12708–12717, 2019. 2
- [34] Paul-Edouard Sarlin, Ajaykumar Unagar, Måns Larsson, Hugo Germain, Carl Toft, Victor Larsson, Marc Pollefeys, Vincent Lepetit, Lars Hammarstrand, Fredrik Kahl, and Torsten Sattler. Back to the Feature: Learning Robust Camera Localization from Pixels to Pose. In *Proceedings of the IEEE/CVF Conference on Computer Vision and Pattern Recognition (CVPR)*, 2021. 2
- [35] T. Sattler, Q. Zhou, M. Pollefeys, and L. Leal-Taixé. Understanding the limitations of cnn-based absolute camera pose regression. In *Proceedings of the IEEE/CVF Conference on Computer Vision and Pattern Recognition (CVPR)*, pages 3297–3307, 2019. 2, 12
- [36] Yoli Shavit and Ron Ferens. Do we really need scene-specific pose encoders? In *Proceedings of the International Conference on Pattern Recognition (ICPR)*, pages 3186–3192. IEEE, 2021. 3, 12
- [37] Yoli Shavit, Ron Ferens, and Yosi Keller. Learning multi-scene absolute pose regression with transformers. In *Proceedings of the IEEE International Conference on Computer Vision (ICCV)*, 2021. 1, 4, 7, 12
- [38] Yoli Shavit, Ron Ferens, and Yosi Keller. Learning multi-scene absolute pose regression with transformers. In *Proceedings of the IEEE International Conference on Computer Vision (ICCV)*, 2021. 3, 4, 6
- [39] Yoli Shavit and Yosi Keller. Camera pose auto-encoders for improving pose regression. In *Proceedings of the European Conference on Computer Vision (ECCV)*, pages 140–157. Springer, 2022. 3
- [40] Jiaming Sun, Zehong Shen, Yuang Wang, Hujun Bao, and Xiaowei Zhou. LoFTR: Detector-free local feature matching with transformers. *Proceedings of the IEEE/CVF*

- Conference on Computer Vision and Pattern Recognition (CVPR)*, 2021. 4
- [41] H. Taira, M. Okutomi, T. Sattler, M. Cimpoi, M. Pollefeys, J. Sivic, T. Pajdla, and A. Torii. Inloc: Indoor visual localization with dense matching and view synthesis. *IEEE Transactions on Pattern Analysis and Machine Intelligence*, pages 1–1, 2019. 2, 12
- [42] Mingxing Tan and Quoc Le. EfficientNet: Rethinking model scaling for convolutional neural networks. volume 97 of *Proceedings of Machine Learning Research*, pages 6105–6114, Long Beach, California, USA, 09–15 Jun 2019. 7
- [43] Akihiko Torii, Relja Arandjelovic, Josef Sivic, Masatoshi Okutomi, and Tomas Pajdla. 24/7 place recognition by view synthesis. In *Proceedings of the IEEE/CVF Conference on Computer Vision and Pattern Recognition (CVPR)*, 2015. 2, 12
- [44] Mehmet Özgür Türkoğlu, Eric Brachmann, Konrad Schindler, Gabriel Brostow, and Áron Monszpart. Visual Camera Re-Localization Using Graph Neural Networks and Relative Pose Supervision. In *Proceedings of the International Conference on 3D Vision (3DV)*. IEEE, 2021. 2, 3, 6, 7, 12
- [45] Ashish Vaswani, Noam Shazeer, Niki Parmar, Jakob Uszkoreit, Llion Jones, Aidan N Gomez, Łukasz Kaiser, and Illia Polosukhin. Attention is all you need. In *Advances in Neural Information Processing Systems (NIPS)*, volume 30, pages 5998–6008, 2017. 4
- [46] F. Walch, C. Hazirbas, L. Leal-Taixé, T. Sattler, S. Hilsenbeck, and D. Cremers. Image-based localization using lstms for structured feature correlation. In *Proceedings of the IEEE International Conference on Computer Vision (ICCV)*, pages 627–637, 2017. 12
- [47] Bing Wang, Changhao Chen, Chris Xiaoxuan Lu, Peijun Zhao, Niki Trigoni, and Andrew Markham. Atloc: Attention guided camera localization. In *Proceedings of the AAAI Conference on Artificial Intelligence (AAAI)*, volume 34, pages 10393–10401, 2020. 12
- [48] J. Wu, L. Ma, and X. Hu. Delving deeper into convolutional neural networks for camera relocalization. In *Proceedings of the IEEE International Conference on Robotics and Automation (ICRA)*, pages 5644–5651, 2017. 3
- [49] Tete Xiao, Mannat Singh, Eric Mintun, Trevor Darrell, Piotr Dollár, and Ross Girshick. Early convolutions help transformers see better. *Advances in Neural Information Processing Systems (NIPS)*, 34:30392–30400, 2021. 4
- [50] Lin Yen-Chen, Pete Florence, Jonathan T. Barron, Alberto Rodriguez, Phillip Isola, and Tsung-Yi Lin. iNeRF: Inverting neural radiance fields for pose estimation. In *Proceedings of the IEEE/RSJ Conference on Intelligent Robots and Systems (IROS)*, 2021. 3
- [51] X. Zhang, H. Xiong, W. Zhou, W. Lin, and Q. Tian. Picking deep filter responses for fine-grained image recognition. In *Proceedings of the IEEE/CVF Conference on Computer Vision and Pattern Recognition (CVPR)*, pages 1134–1142, 2016. 4
- [52] Qunjie Zhou, Torsten Sattler, Marc Pollefeys, and Laura Leal-Taixé. To learn or not to learn: Visual localization from essential matrices. In *Proceedings of the IEEE International Conference on Robotics and Automation (ICRA)*, pages 3319–3326. IEEE, 2020. 2, 3, 6, 12
- [53] Yi Zhou, Connelly Barnes, Jingwan Lu, Jimei Yang, and Hao Li. On the continuity of rotation representations in neural networks. In *Proceedings of the IEEE/CVF Conference on Computer Vision and Pattern Recognition (CVPR)*, pages 5745–5753, 2019. 2, 3, 5, 8, 13

Table 4: Cross-Comparison of different localization methods in previously seen and unseen environments. We consider representative methods from five localization families, which present different runtime and storage requirements (indicated as low/intermediate/high with '+'/'++'/'+++'), respectively) and vary in their ability to learn multiple scenes with a single model (Multi-Scene) and to generalize to unseen scenes (Generalization), which we indicate with a  $\checkmark$  sign. For each method, we provide the reported average of median position and orientation errors (in meters/degrees, respectively) for seen and unseen localization on the 7Scenes dataset. For RPR methods, we report seen and unseen statistics in the same manner as in Tables 1 and 2. We report the performance of IR and SLP methods, which were trained on different large datasets, in the Unseen category. Results marked with \* were reported and reproduced by [44]. The 'F' character in the Unseen column indicates that the method fails to localize in unseen scenes.

Method	Family	Storage	Runtime	Multi-Scene	Generalization	Seen	Unseen
DenseVLAD[43]	IR	++	++	$\checkmark$	$\checkmark$	–	0.26/12.5
DenseVLAD+inter.[35]	IR	++	++	$\checkmark$	$\checkmark$	–	0.24/11.7
InLoc[41]	SLP	+++	+++	$\checkmark$	$\checkmark$	–	0.04/1.44
DSAC[6]	SCR	+	+			0.20/6.30	F
DSAC++[7]	SCR	+	+			0.08/2.40	F
DSAC*[8]	SCR	+	+			0.03/1.40	F
PoseNet[25]	APR	+	+			0.44/10.4	F
BayesianPN[23]	APR	+	+			0.47/9.81	F
LSTM-PN[46]	APR	+	+			0.31/9.85	F
IRPNet[36]	APR	+	+			0.23/8.49	F
PoseNetLearn[24]	APR	+	+			0.24/7.87	F
GeoPoseNet[24]	APR	+	+			0.23/8.12	F
Atloc[47]	APR	+	+			0.20/7.56	F
MSPN[5]	APR	+	+	$\checkmark$		0.20m/8.41	F
MS-Transformer[37]	APR	+	+	$\checkmark$		0.18/7.28	F
NN-Net[26]	RPR	++	++	$\checkmark$	$\checkmark$	0.21/9.30	2.31/13.0*
EssNet[52]	RPR	++	++	$\checkmark$	$\checkmark$	0.22/8.00	0.89/40.2*
NCEssNet[52]	RPR	++	++	$\checkmark$	$\checkmark$	0.21/7.50	0.82/26.2*
RelPoseGNN[44]	RPR	++	++	$\checkmark$	$\checkmark$	0.16/5.20	0.36/13.6
<b>Relformer (Ours)</b>	RPR	++	++	$\checkmark$	$\checkmark$	0.18/6.27	0.34/9.72

Table 5: **Ablations of our network architecture on previously seen scenes.** We report the median position and orientation errors (in meters and degrees, respectively) for each scene and the average of medians across all scenes. Performance is reported for a baseline architecture and when extracting Feature Maps (FM), aggregating them with a Transformer Encoder (TE) and when learning a 6D vector to recover the rotation matrix through orthogonalization (6D).

FM	TE	6D	Chess	Fire	Heads	Office	Pumpkin	Kitchen	Stairs	Average
			0.10/4.79	0.34/11.7	0.14/11.0	0.15/6.00	0.19/4.67	0.18/5.86	0.26/8.86	0.20/7.57
$\checkmark$			0.10/5.95	0.22/10.7	0.18/12.9	0.18/7.08	0.18/6.24	0.189/7.05	0.29/10.2	0.19/8.58
$\checkmark$	$\checkmark$		0.10/4.92	0.23/8.72	0.15/11.8	0.16/5.46	0.17/4.21	0.18/5.20	0.24/7.78	0.18/6.87
$\checkmark$	$\checkmark$	$\checkmark$	0.11/4.01	0.23/8.57	0.17/10.89	0.16/4.92	0.15/4.15	0.19/4.89	0.24/6.46	0.18/6.27

Table 6: **Ablations of our network architecture on unseen scenes.** We report the median position and orientation errors (in meters and degrees, respectively) for each scene and the average of medians across all scenes, when training with sets of six scenes and evaluating on the remaining scene. Performance is reported for a baseline architecture and when extracting Feature Maps (FM), aggregating them with a Transformer Encoder (TE) and when learning a 6D vector to recover the rotation matrix through orthogonalization (6D).

FM	TE	6D	Chess	Fire	Heads	Office	Pumpkin	Kitchen	Stairs	Average
			0.30/11.8	0.36/15.5	0.27/15.25	0.35/10.8	0.37/11.8	0.34/11.8	0.45/19.9	0.35/13.8
✓			0.32/10.2	0.37/15.1	0.22/13.6	0.33/10.3	0.38/12.9	0.36/11.7	0.40/13.0	0.34 /12.4
✓	✓		0.27/8.80	0.35/12.0	0.25/12.6	0.30/7.94	0.36/8.17	0.32/8.36	0.42/10.1	0.32/9.71
✓	✓	✓	0.27/8.50	0.34/10.4	0.28/12.1	0.32/8.24	0.40/9.06	0.32/9.23	0.425/10.5	0.34/9.72

Table 7: **Ablations of the backbone by localizing previously seen and unseen environments.** We report the median position and orientation errors (in meters and degrees, respectively) for the Fire scene (7scenes dataset), when the scene data is included in (Seen) or excluded from (Unseen) the training data.

Backbone	Dimension	Seen (Fire)	Unseen (Fire)
ResNet34	$7 \times 7 \times 512$	0.32/14.2	0.39/15.2
ResNet50	$7 \times 7 \times 2048$	0.27/13.3	0.42/15.8
EfficientNet-B0	$7 \times 7 \times 320$	0.24/11.8	0.34/11.6

Table 8: **Ablations of feature maps and aggregation operators on the 7Scenes dataset.** We report the average of median position and orientation errors (in meters and degrees, respectively) when varying on the type of aggregation (Agg.) and the dimensions of the feature maps.

Agg.	Feature Maps	Average
2D Conv	$7 \times 7 \times 320 / 14 \times 14 \times 112$	0.19/8.15
2D Conv	$14 \times 14 \times 112 / 28 \times 28 \times 40$	0.19/8.59
Transformer Encoder	$7 \times 7 \times 320 / 14 \times 14 \times 112$	0.18/7.35
Transformer Encoder	$14 \times 14 \times 112 / 28 \times 28 \times 40$	0.18/6.87

Table 9: **Ablations of rotation representation (7Scenes).** We compare the performance when learning with different rotation representations (Repr.): Quaternion (Quat.), 6D and 9D. We report the median position and orientation errors (in meters and degrees, respectively) for each scene and the average of error medians across all scenes.

Repr.	Chess	Fire	Heads	Office	Pumpkin	Kitchen	Stairs	Average
Quat.	0.10/4.92	0.23/8.72	0.15/11.8	0.16/5.46	0.17/4.21	0.18/5.20	0.24/7.78	0.18/6.87
9D [27]	0.11/4.66	0.23/9.24	0.17/11.8	0.16/5.13	0.17/3.99	0.19/4.83	0.26/8.25	0.18/6.84
6D [53]	0.11/4.01	0.23/8.57	0.17/10.89	0.16/4.92	0.15/4.15	0.19/4.89	0.24/6.46	0.18/6.27